Astrochemistry VII – Through the Cosmos
from Galaxies to Planets
Proceedings IAU Symposium No. 332, 2017
M. Cunningham, T. Millar & Y. Aikawa, eds.

doi:10.1017/S174392131700686X

Dust formation at cryogenic temperatures

Thomas Henning[1], Cornelia Jäger[2], Gaël Rouillé[2], Daniele Fulvio[3] and Serge A. Krasnokutski[2]

[1]Max Planck Institute for Astronomy, Königstuhl 17, 69117 Heidelberg, Germany
email: henning@mpia.de

[2]Laboratory Astrophysics Group of the Max Planck Institute for Astronomy at the Friedrich Schiller University Jena, Institute of Solid State Physics, Helmholtzweg 3, 07743 Jena, Germany

[3]Departamento de Física, Pontifícia Universidade Católica do Rio de Janeiro, Rua Marquês de São Vicente 225, 22451-900 Gávea, Rio de Janeiro, RJ Brazil

Abstract. The efficiency of dust formation in a variety of environments is an ongoing topic for discussions, especially if it comes to dust formation in the interstellar medium. Although this possibility is discussed in a wide range of numerical studies, experiments on the formation of dust at low densities and temperatures are mostly lacking. This contribution summarizes the main findings of our low-temperature condensation experiments including the formation of silica, complex silicates with pyroxene and olivine stoichiometry, and of carbonaceous refractory materials. Atomic and molecular species to be expected as products of supernovae shock fronts were produced by laser ablation of silicates and graphite. These species were deposited together with a rare gas on cold substrates representing the surfaces of surviving dust grains in the interstellar medium. After characterizing the precursor species, the rare gas matrix was annealed to induce diffusion and reactions between the initial components. We found the production of amorphous and homogeneous silica and magnesium iron silicates at temperatures of about 12 K in a barrierless reaction as monitored by infrared spectroscopy. The 10 μm band of the low-temperature siliceous condensates shows a striking similarity to the 10 μm band of interstellar silicates. Carbonaceous atoms and molecules can also react without a barrier and form an amorphous or hydrogenated amorphous carbon material. The refractory condensate has properties comparable to fullerene-like carbon grains formed at high temperatures.

Keywords. Cosmic Dust, Dust Formation, Cosmic Silicates, Laboratory Data

1. Introduction

Asymptotic giant branch (AGB) stars and supernovae (SNe) have been considered as the main dust factories in our and other galaxies. However, the freshly formed stardust is destroyed by SNe shocks. Models of the multi-phase interstellar medium (ISM) indicate that only a small fraction of the stardust survives the destructive processes and dust should be reformed efficiently in the denser phases of the ISM (Zhukovska, Gail & Trieloff 2008, Draine 2009, Zhukovska & Henning 2013). The importance of dust growth by the accretion of gas-phase metals was also demonstrated by recent cosmological simulations (McKinnon, Torrey & Vogelsberger 2016, Zhukovska *et al.* 2016). Aoyama *et al.* (2017) investigated the time evolution and spatial distribution of dust in an isolated galaxy and found that small grain production by shattering triggers accretion and coagulation. This process becomes significant at ages of about 1 Gyr after a large amount of small grains are produced by shattering. Michałowski (2015) derived dust yields for AGB stars and SNe required to explain dust masses of galaxies at $z = 6.3$–7.5 for which dust emission has been detected. The detected dust mass cannot be produced by AGB stars and SNe and suggests an efficient grain growth process in the ISM at these early epochs.

In the ISM, refractory atoms and molecules generated by the erosion of grains in SNe shocks can be re-accreted onto surviving grains. This process is thought to occur at low temperatures roughly between 10 and 20 K. Since all circumstellar and SNe-formed dust grains are mixed in the ISM, interstellar destruction processes such as sputtering and grain-grain shattering should produce carbonaceous and siliceous molecular and atomic precursor species. In order to provide an experimental basis for dust formation in the ISM, we performed dedicated laboratory experiments with the goal to study the condensation of major dust components including silicates and carbonaceous grains. We summarize the experimental setup and discuss the results of low-temperature condensation in differently doped cryogenic matrices.

2. Experimental methods

Laser ablation of cosmic dust analogs was used to simulate the destructive effect of SNe-induced shocks on siliceous and carbonaceous refractory dust grains. The resulting small molecules and atoms act as the precursors of dust formation. Polycrystalline graphite and amorphous silicates such as Mg_2SiO_4 (forsterite stoichiometry) and $Mg_{0.4}Fe_{0.6}SiO_3$ (pyroxene stoichiometry) synthesized by melting and quenching were used as targets for laser ablation. The experiment was carried out using a pulsed laser source emitting photons with a wavelength of 532 nm corresponding to a power density of 2 to 4 GW cm^{-2}. In a first step, the vaporized species were isolated in Ar or Ne matrices and deposited on cold KBr substrates (10 K) simulating the dust surface in space. Infrared (IR) and UV/VIS (ultraviolet/visible) spectra were recorded in situ providing the opportunity to identify the laser-vaporized species.

In a second step, the matrices were annealed by increasing the temperature ($\Delta T = 4$–6 K). The annealing process is performed in such a way that most of the matrix material remains intact. The annealing was applied to trigger the diffusion of species within the rare-gas matrix leading to collisions between the precursor species. After only a few minutes, the matrix was cooled down again to perform UV/VIS and IR spectroscopy and to monitor the formation of larger species or refractory grains. The final phase of the experiment consists of the heating of the substrate, the evaporation of the matrix, and the characterization of the material located on the substrate. The characterization of the produced refractory material was performed by high-resolution electron microscopy (HRTEM), and energy-dispersive X-ray (EDX) spectroscopy. The entire experiment is schematically described in Figure 1. Details of the experiments are summarized by Rouillé *et al.* (2013), Krasnokutski *et al.* (2014), Rouillé *et al.* (2014), and Fulvio *et al.* (2017).

Another experimental approach to study chemical reactions and the condensation of refractory materials at temperatures lower than 10 K is provided by helium droplets doped with a variety of species. The He droplet setup was described by (Krasnokutski, Rouillé & Huisken (2005)). The experiment consists of three differentially pumped chambers. In the source chamber, large He clusters are generated by supersonic expansion of He gas at $p = 20$ bar through a liquid He-cooled pinhole nozzle. In the second chamber, the He droplets can be doped with astrophysically relevant species. The gas-phase species are picked up by the He nanodroplets and carried to the third chamber, which is equipped with an electron bombardment ionizer and a quadrupole mass spectrometer. The temperature of the He droplets is 0.37 K and reactions inside occur under equilibrium conditions. The liquid He droplets serve as the cold reaction surface. The reaction energy between individual species can be experimentally determined using a calorimetric

https://doi.org/10.1017/S174392131700686X Published online by Cambridge University Press

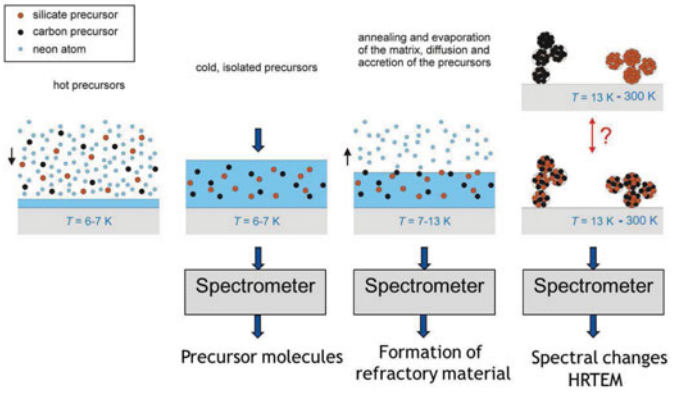

Figure 1. A sketch of the experimental procedure applied to study the cold condensation of silicates, carbonaceous grains, and mixed systems.

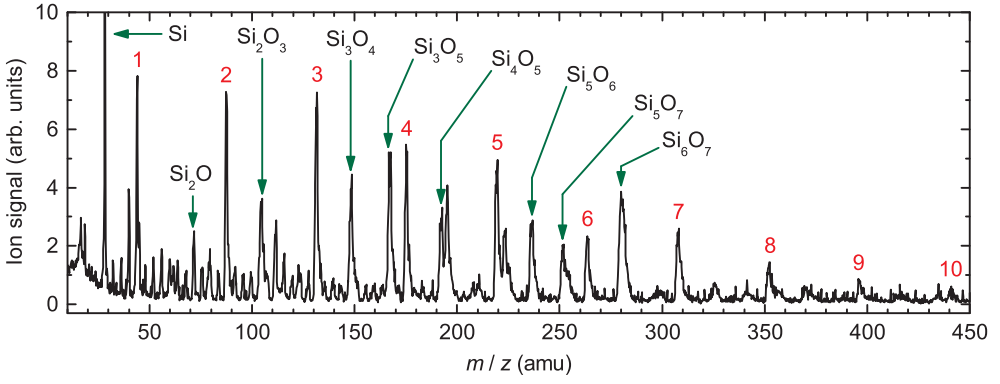

Figure 2. Mass spectrum of He droplets doped with SiO and H_2O molecules. The mass peaks corresponding to $(SiO)_k$ clusters are labeled with the corresponding index k. The data are from Krasnokutski *et al.* (2014).

approach in which the amount of evaporated He atoms can be converted into the reaction energy (Krasnokutski *et al.* 2014).

3. Low-temperature condensation of SiO_2 and complex silicates

SiO molecules are the main precursors for silicates in evolved stars (Gail & Sedlmayr 1999) and SiO_2 represents a major component of the solid silicates. Therefore, the experimental work primarily focused on the condensation of solid SiO_x materials at low temperature using the He droplet technique and the matrix approach. Figure 2 presents the mass spectrum recorded after doping He droplets with SiO and H_2O molecules. The mass peaks are attributed to various Si_xO_y clusters, including $(SiO)_k$ clusters. The energies of SiO polymerization reactions have been determined experimentally with the calorimetric method and compared to calculations based on the density functional theory. Both results confirmed the formation of cyclic $(SiO)_k$ $(k = 2 - 3)$ clusters inside the He droplets. The SiO molecules react without an energy barrier and thus, oligomerization and formation of large molecules were found to be efficient. Such reactions can be expected on the surface of cold dust grains.

The results obtained in He droplets were confirmed by condensation studies in Ne matrices at around 10K. UV/VIS and IR spectroscopy were performed of a SiO-doped

https://doi.org/10.1017/S174392131700686X Published online by Cambridge University Press

Ne matrix at different annealing temperatures. $(SiO)_x$ oligomers (x = 1–3) identified in the cryogenic matrix disappeared during annealing of the Ne matrix up to 11 K and a broad band at about 9.5 μm characteristic of Si–O stretching vibrations in solid SiO_2 appeared. HRTEM and EDX spectroscopy revealed a homogeneous, amorphous structure and a SiO stoichiometry.

Apart from the simple SiO_x system, the successful condensation of complex silicates with pyroxene, olivine, and nonstoichiometric composition at low temperatures was also experimentally studied in cryogenic matrices. Two different silicates corresponding to Mg_2SiO_4 and $Mg_{0.4}Fe_{0.6}SiO_3$ (olivine and pyroxene) were used to produce refractory molecular and atomic species.

Spectroscopy in the UV/VIS and IR range was employed to identify the deposited species in the cryogenic matrices. Fe and Mg atoms were detected in the UV range demonstrating an efficient formation of Mg and Fe from the silicate targets. IR absorption bands point to the presence of O_3 (1039 cm^{-1}), O_4^+ (1164 cm^{-1}), and SiO (1228 cm^{-1}) in the matrix. Absorption features due to a complex possibly involving H_2 and H_3O^+ or $H_2O_5^+$ were also detected (Jacox & Thompson 2013). Based on comparisons with measurements on species isolated in Ar matrices, we assigned tentatively the bands at 1369 and 1424 cm^{-1} to SiO_3 and SiO_2, respectively (Tremblay *et al.* 1996). In addition, FeO (870 cm^{-1}) (Green, Reedy & Kay 1979) and OFeO (950 cm^{-1}) (Chertihin *et al.* 1996) could be identified.

IR spectroscopy is the most efficient method to monitor the condensation of silicates in the ice as a function of the temperature. Figure 3a shows the spectra of the material obtained by the condensation of species produced in the laser ablation of the Mg_2SiO_4 target. The spectrum was measured after the annealing of the doped Ne matrix to temperatures of 13 K and subsequent cooling to 6.5 K. Beside the features due to CO, CO_2, and H_2O, a band at 1000 cm^{-1} was recorded that is characteristic for a silicate of amorphous structure. The profile of this band is slightly affected by the presence of the water ice feature at around 780 cm^{-1} (Öberg *et al.* 2007). After warming up to room temperature, the position of the Si–O absorption band could be found at ≈1020 cm^{-1} (9.8 μm). Similar results were obtained with the $Mg_{0.4}Fe_{0.6}SiO_3$ target.

Figure 3b compares the IR spectra of the condensates obtained from the pure Mg- and the Mg-Fe-silicate targets to the interstellar silicate absorption feature. The Mg-Fe silicate shows a band at ≈990 cm^{-1} (10.1 μm). Similar band positions demonstrate that both condensates must have comparable stoichiometry even though different targets were used. The EDX analysis revealed the final non-stoichiometric compositions $Mg_{0.3}Fe_{0.9}SiO_{3.6}$ and $MgSiO_{2.8}$ for the condensates. This behavior was caused by a non-equal evaporation of Mg and Fe from the original silicate targets during the laser vaporization. HRTEM images of the $Mg_{0.3}Fe_{0.9}SiO_{3.6}$ condensate show fluffy aggregates composed of nanometer-sized, amorphous grains (see Fig. 4). This structure is also typical of the condensed $MgSiO_{2.8}$ material. No phase separations into individual oxides such as FeO, MgO, and SiO_2 are observed.

4. Low-temperature condensation of carbonaceous materials

The formation of a carbonaceous refractory condensate from molecular precursors was observed after deposition on a cold substrate at about 10 K (with or without Ar matrix). The isolation of the laser ablated carbonaceous species in an Ar matrix provided information on the precursor molecules that eventually form the refractory material. Beside the presence of species such as H_2O, CO, CO_2, C_3O, water clusters, various isolated odd- and even-numbered carbon chains were detected in the UV/VIS and IR ranging from

https://doi.org/10.1017/S174392131700686X Published online by Cambridge University Press

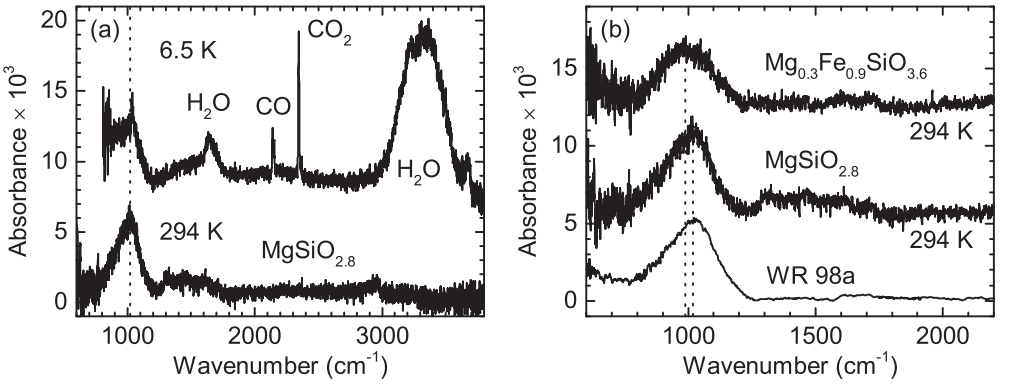

Figure 3. (a) IR spectra of the $MgSiO_{2.8}$ condensate. The top spectrum was measured at 6.5 K and the bottom spectrum was recorded at room temperature after sublimation of ices. (b) IR features of the silicate condensates obtained with the Mg_2SiO_4 and $Mg_{0.4}Fe_{0.6}SiO_3$ targets compared to the normalized silicate absorption feature toward WR 98a representing the local ISM (Chiar & Tielens 2006). The spectra were vertically shifted for clarity. The data are from Rouillé *et al.* (2014).

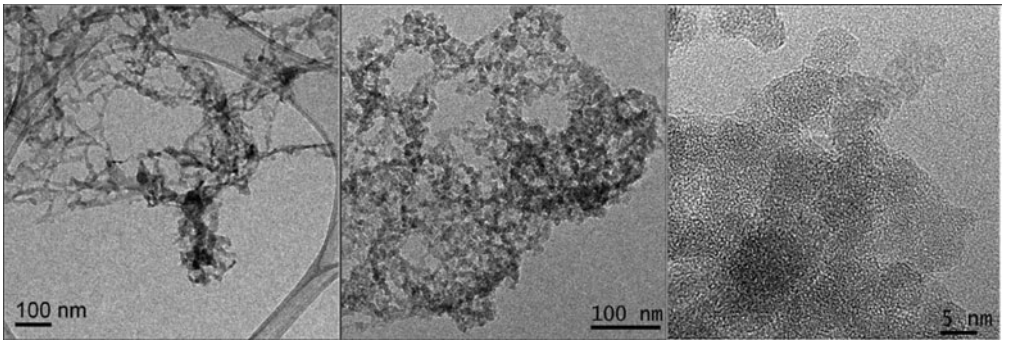

Figure 4. HRTEM image of the $Mg_{0.3}Fe_{0.9}SiO_{3.6}$ condensate prepared by the evaporation and recondensation of a magnesium iron silicate at about 10 K. The right image allows a direct view insight the amorphous grains whereas the two left images show the fluffy morphology of the condensate.

C_2 up to C_{13}. After the warming up of the cryogenic ice layer to room temperature, a refractory residue remained on the substrate.

Simultaneous deposition of carbonaceous species by laser ablation of graphite and molecular hydrogen in the Ar ice layer led to the formation of small hydrocarbon molecules such as C_2H_2, C_4H_2, $C_2H_2 \cdot H_2O$.

The carbonaceous species in pure and hydrogen-containing Ar matrices react between each other without an energy barrier resulting in the formation of a refractory carbonaceous material. IR spectra of the carbonaceous condensate at different temperatures are depicted in Fig. 5. Already at a low temperature of about 10 K, a decrease of the IR transmission with increasing ablation time can be observed. This is caused by the growth of a refractory carbonaceous film, which is characterized by free charge carriers responsible for a continuous absorption from the UV up to the MIR and weak scattering effects at small wavelengths. The increasing extinction is also accompanied by the occurrence of a broad plateau band between 1000 and 1400 cm^{-1}. The formation of such a plateau is a feature of amorphous and hydrogenated amorphous carbon samples prepared by gas-phase condensation techniques (Jäger, Mutschke & Henning 1998, Schnaiter *et al.* 1998,

https://doi.org/10.1017/S174392131700686X Published online by Cambridge University Press

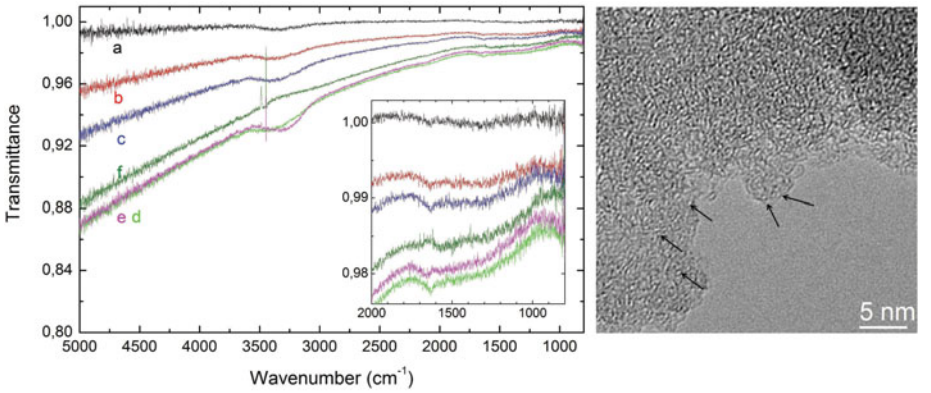

Figure 5. Left: Spectral evolution of the carbonaceous condensate formed at 10 K with increasing deposition time and after warming up to 200 K. Curves a, b, c, and d correspond to 5, 15, 25, and 35 min laser ablation at about 10 K. Curves e and f represent the warming up to 40 K and 200 K, respectively. Right: HRTEM micrograph of the internal structure of the condensed carbon material in Ar matrix. Fullerene-like carbon structures are visible such as small bucky onions and strongly bent graphene layers. Individual fullerene molecules of various sizes and shapes are identified and marked with arrows. The data are from Fulvio *et al.* (2017).

Llamas-Jansa *et al.* 2007). The broad absorption is a mixture of vibrational bands of various functional groups such as ν_{C-O-C}, ν_{C-C}, and δ_{C-H}. More details on the identification of individual species in the Ar ice matrix are provided in Fulvio *et al.* (2017).

The condensation of carbonaceous species at temperatures around 10 K provide similar fullerene-like carbon structures (see Fig. 5) as produced in high temperature condensation processes (Jäger *et al.* 2009). The presence of differently sized cage molecules, strongly bent graphene layers, and individual fullerenes can be observed in the images. The high-temperature formation pathway was initiated by the formation of chain-like structures that are formed as intermediates and finally convert into cage-like structures including fragments and completely closed cages. At low temperatures, the condensation process is also governed by carbon chains that grow and finally convert into more stable aromatic structures with the characteristic curved graphene layers.

5. Low-temperature condensation of of siliceous and carbonaceous materials

One of the challenges for interstellar dust models is the question if silicates and carbonaceous grains are two distinct dust populations or form Si-C-based compounds. Laboratory experiments to investigate the formation of refractory components in matrices containing both types of species were started. First experiments were dedicated to study possible reactions between carbonaceous and SiO_x species. Two different targets were used for the laser ablation process. SiO and carbon species such as C_2, C_3, C_n were deposited in a Ne matrix. After activation of the diffusion by moderate annealing to 9-11 K, we observed the rise of a band at 10 μm. This clearly indicates the appearance of a refractory SiO_x condensate in the remaining Ne ice. No hints on the formation of other components could be identified spectroscopically. After warming up, the condensate was studied by HRTEM and EDX analysis. A solid, refractory SiO component was found to be spatially separated from carbonaceous grains (see Fig. 6).

The results clearly point to a separate formation of carbonaceous and siliceous refractory materials. The formation of SiC was not observed in the condensate. Yet, small

https://doi.org/10.1017/S174392131700686X Published online by Cambridge University Press

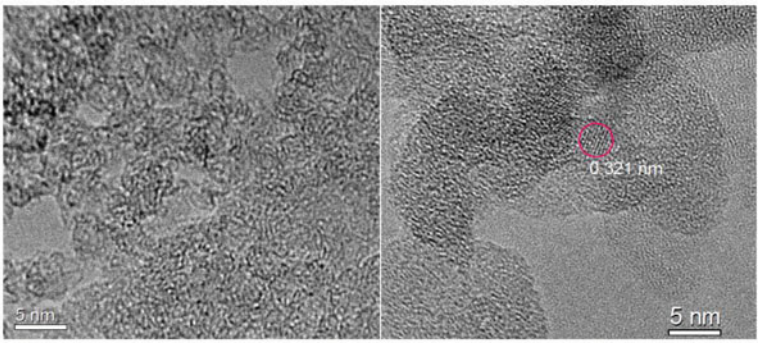

Figure 6. HRTEM images of carbonaceous (left) and SiO_x grains (right) condensed in a Ne ice containing siliceous and carbonaceous species prepared by simultaneous laser ablation of a graphite and a SiO target. Both materials are characterized by an amorphous structure. The silicate on the right sight contains a few small crystalline inclusions of about 2 nm that were identified as silicon based on the distances between their lattice fringes.

inclusions of silicon (∼2 nm) were detected in the SiO_x grains. These silicon inclusions were probably formed by the reductive effect of the carbon species on SiO resulting in a oxygen-deficient SiO material. Further experiments on the simultaneous condensation of complex silicates and carbonaceous refractory material are still under progress but all results so far confirm the separation of silicates and carbonaceous grains.

6. Astrophysical implications and conclusions

In the denser ISM, gaseous species accrete on cold surfaces of pre-existing small particles. To simulate such processes in the laboratory, we have evaporated dust analogs that have successfully been used to model spectral energy distributions of many astrophysical sources (Gielen *et al.* 2011, Min *et al.* 2007). Important precursors for silicates such as Si, SiO, FeO, Mg, and Fe produced in our experiments were already observed in the ISM (Schilke *et al.* 1997, Walmsley *et al.* 2002, Furuya *et al.* 2003).

We detected a barrierless formation of amorphous and homogeneous silica and magnesium iron silicates at temperatures of about 12 K. The morphology and structure of the condensates are remarkably similar to those silicates produced by gas-phase condensation at high temperature. Both types of condensates are of amorphous structure and show very similar spectral properties comparable to the interstellar 10 μm absorption band. Distinct structural and spectral differences between high- and low-temperature condensates could not be identified.

Carbonaceous atoms and molecules also react without a barrier and form an amorphous or hydrogenated amorphous carbon material. One of the amazing findings of this study is the observation of fullerene-like carbon structures condensing at temperatures of about 10 K. The chemical evolution into fullerene-like carbon materials containing fullerene molecules of different sizes and shapes indicates a formation pathway via long and branched carbon chain molecules that eventually convert into aromatic structures even at temperatures around 15 K (Yamaguchi & Wakabayashi 2004). Such a process was predicted and observed for high-temperature condensation processes by Cherchneff *et al.* (2000) and by Jäger *et al.* (2009).

Experiments on the doping of cryogenic matrices with both carbonaceous and siliceous species show the condensation of distinct carbonaceous and silicate grains. No silicon carbide was detected. The formation of small crystalline Si inclusions could be observed

https://doi.org/10.1017/S174392131700686X Published online by Cambridge University Press

in the SiO_x grains. These were formed by the reduction of silicon with carbon species leading to the oxidation of small carbon clusters or molecules.

References

Aoyama, S., Hou, K.-C., Shimizu, I., Hirashita, H., Todoroki, K., Choi, J.-H., & Nagamine, K. 2017, *MNRAS*, 466, 105

Draine, B. T. 2009, in: Th. Henning, E. Grün & J. Steinacker (eds.), *Cosmic Dust Near and Far*, ASP Conf. Ser. Vol. 414 (San Francisco: ASP), p. 453

Cherchneff, I., Le Teuff, Y. H., Williams, P. M., & Tielens, A. G. G. M. 2000, *A&A*, 357, 572

Chertihin, G. V., Saffel, W., Yustein, J. T., Andrews, L., Neurock, M., Ricca, A., & Bauschlicher, C. W. 1996, *J. Phys. Chem.*, 100, 5261

Chiar, J. E. & Tielens, A. G. G. M. 2006, *ApJ*, 637, 774

Fulvio, D., Gobi, S., Jäger, C., Kereszturi, A., & Henning, Th. 2017, *ApJS*, 233, 14

Furuya, R. S., Walmsley, C. M., Nakanishi, K., Schilke, P., & Bachiller, R. 2003, *A&A*, 409, L21

Gail, H.-P. & Sedlmayr, E. 1999, *A&A*, 347, 594

Gielen, C., Bouwman, J., Van Winckel, H., Lloyd Evans, T., Woods, P. M., Kemper, F., Marengo, M., Meixner, M., Sloan, G. C., & Tielens, A. G. G. M. 2011, *A&A*, 533, A99

Green, D. W., Reedy, G. T., & Kay, J. G. 1979, *J. Mol. Spectrosc.*, 78, 257

Jacox, M. E. & Thompson, W. E. 2013, *J. Phys. Chem. A*, 117, 9380

Jäger, C., Huisken, F., Mutschke, H., Llamas Jansa, I., & Henning, Th. 2009, *ApJ*, 696, 706

Jäger, C., Mutschke, H., & Henning, Th. 1998, *A&A*, 332, 291

Krasnokutski, S., Rouillé, G., & Huisken, F. 2005, *Chem. Phys. Lett.*, 406, 386

Krasnokutski, S. A., Rouillé, G., Jäger, C., Huisken, F., Zhukovska, S., & Henning, Th. 2014, *ApJ*, 782, 15

Llamas-Jansa, I., Jäger, C., Mutschke, H., & Henning, Th. 2007, *Carbon*, 45, 1542

McKinnon, R., Torrey, P., & Vogelsberger, M. 2016, *MNRAS*, 457, 3775

Michałowski, M. 2015, *A&A*, 577, A80

Min, M., Waters, L. B. F. M., de Koter, A., Hovenier, J. W., Keller, L. P., & Markwick-Kemper, F. 2007, *A&A*, 462, 667

Öberg, K. I., Fraser, H. J., Boogert, A. C. A., Bisschop, S. E., Fuchs, G. W., van Dishoeck, E. F., & Linnartz, H. 2007, *A&A*, 462, 1187

Rouillé, G., Jäger, C., Krasnokutski, S. A., Krebsz, M., & Henning, T. 2014, *Faraday Discuss.*, 168, 449

Rouillé, G., Krasnokutski, S. A., Krebsz, M., Jäger, C., Huisken, F., & Henning, T. 2013, in: A. Andersen, M. Baes, H. Gomez, C. Kemper & D. Watson (eds.), *The Life Cycle of Dust in the Universe: Observations, Theory, and Laboratory Experiments*, PoS(LCDU2013) (Proceedings of Science), p. 47

Schilke, P., Walmsley, C. M., Pineau des Forêts, G., & Flower, D. R. 1997, *A&A*, 321, 293

Schnaiter, M., Mutschke, H., Dorschner, J., Henning, Th., & Salama, F. 1998, *ApJ*, 498, 486

Tremblay, B., Roy, P., Manceron, L., Alikhani, M. E., & Roy, D. 1996, *J. Chem. Phys.*, 104, 2773

Walmsley, C. M., Bachiller, R., Pineau des Forêts, G., & Schilke, P. 2002, *ApJ*, 556, L109

Yamaguchi, Y. & Wakabayashi, T. 2004, *Chem. Phys. Lett.*, 388, 436

Zhukovska, S., Dobbs, C., Jenkins, E. B., & Klessen, R. S. 2016, *ApJ*, 831, 147

Zhukovska, S., Gail, H.-P., & Trieloff, M. 2008, *A&A*, 479, 453

Zhukovska, S. & Henning, T. 2013, *A&A*, 555, A99